Int. J. Nano Dimens., 13 (3): 282-295, Summer 2022

ORIGINAL ARTICLE

Sheet-like Iron Hydroxyl Phosphate as an effective flame retardant and smoke suppressant for Polyacrylonitrile

*Taher Rahimi-Aghdam, Zahra Shariatinia**

Department of Chemistry, Amirkabir University of Technology (Tehran Polytechnic), 15875-4413, Tehran, Iran.

Received 03 April 2022; revised 29 April 2022; accepted 09 May 2022; available online 15 May 2022

Abstract

A novel, one-step, facile and low-cost strategy was successfully designed to synthesize iron hydroxyl phosphate (IP) nanosheets via solvothermal method using iron (II) sulfate heptahydrate, ethylene glycol, and phosphoric acid. Then, for the first time, the flame retardant and smoke suppressant properties of the IP were studied. The synthesized IP nanosheets were added into the polyacrylonitrile (PAN) matrix, by a solvent blending method, to prepare PAN/IP nanocomposite. The structure and morphology of the IP nanosheets were carefully characterized by X-ray diffraction (XRD), X-ray photoelectron spectrum (XPS), Fourier-transform infrared (FT-IR) spectroscopy, Raman spectroscopy, field emission scanning electron microscopy (FE-SEM) and transmission electron microscopy (TEM). In addition, the thermal stability, flame retardancy and fire hazard of the PAN/IP nanocomposite were investigated by thermogravimetric analysis (TGA), cone calorimetry, and UL-94 vertical burning test. The PAN/IP nanocomposite exhibited significantly higher smoke suppression and flame retardancy capability as well as less fire hazards than those of the pure PAN. Moreover, incorporation of the IP into the PAN matrix increased the residual char. These improvements were attributed to the ability of the IP to contribute in formation of effective barrier char layer on the PAN, sheet-like morphology of the IP as well as catalytic activity of the IP in carbon monoxide (CO) oxidation.

Keywords: *Char Barrier Layer; Fire Hazard; Flame Retardant; Iron Hydroxyl Phosphate Nanosheets; Polyacrylonitrile; Smoke Suppressant.*

How to cite this article

Rahimi-Aghdam t., Shariatinia Z. Sheet-like Iron Hydroxyl Phosphate as an effective flame retardant and smoke suppressant for Polyacrylonitrile. Int. J. Nano Dimens., 2022; 13(3): 282-295.

INTRODUCTION

The flammability and combustibility of polymeric materials are major shortcomings limiting their applications and require more new environmentally benign solutions [1]. Fire hazards of polymers can be considered as two categories including thermal and non-thermal hazards. The thermal hazards are related to the amount of heat that is released during the combustion of the polymer which is a key factor in the spread of fire [2]. Thermal hazards can be investigated by heat release rate (HRR) or more precisely by peak heat release rate (PHRR) using the cone calorimetry analysis [1, 3]. The lower the HRR (or PHRR), the higher is the fire safety. The non-thermal hazards are caused by smoke as well as toxic and non-toxic gases [3-5]. Smoke and micrometer-sized particles produced during the fire impair the visibility of victims and may have poisoning effects [3]. In addition, narcotic effect of toxic gases, especially CO, prevents recognizing possible escape ways by most fire victims [3, 6]. Thus, increasing the overall fire safety of polymers requires prevention of their flammability in addition to avoiding production of toxic gases and smoke.

Due to its valuable characteristics including radiation and light resistance, dyeability, elasticity and flexibility, polyacrylonitrile (PAN) has broadly been used by textile industries [3, 4, 7]. However, its low limiting oxygen index, LOI (~18%), severe melt-dripping and high smoke quantity released

* Corresponding Author Email: *shariati@aut.ac.ir*

throughout its combustion increase fire hazards which induce the need to improve the flame retardancy of PAN [4].

Two groups of flame-retardants that have recently attracted attention are two-dimensional (2-D) structures and phosphorous containing materials. Incorporation of phosphorous-based flame retardants into a polymer matrix can reinforce the material and enhance the char layer strength that thereby a protective barrier layer is formed on the polymer surface; hence, the heat and mass transfer processes can be interrupted during the combustion of polymeric nanocomposites [8-12]. Furthermore, phosphorous catalyzes the carbonization process which causes more effective barrier influence [11]. For instance, Wang *et al.* prepared a nanocomposite of α-zirconium phosphate and poly(ethylene terephthalate) (PET) through in situ polymerization and showed that the α-zirconium phosphate nanostructures improved the flame retardancy of the PET [13]. Zhang *et al.* used hydroxylamine hydrochloride to modify the PAN fabric. Then, amidoxime PAN fabric was prepared that was further modified by phosphorylation in presence of phosphoric acid affording a flame retardant PAN material [14]. The glycidyl methacrylate was grafted onto the PAN which was further modified using phosphorus acid and hydrazine hydrate to prepare a PAN with the flame retardant property [8]. Moreover, a great deal of attention has been paid to 2-D organic and inorganic materials like bare and modified graphene [15, 16], graphitic carbon nitride [17], montmorillonite [18] and layered double hydroxides (LDH) [19] as flame retardants. In addition to composition-related flame retardant properties of mentioned materials, the 2-D morphology has an important role on improving the flame retardancy effect [16, 17]. Hu *et al.* functionalized the graphene oxide (GO) by N-aminoethyl piperazine and phosphonate derivative to study the flame retardancy and smoke suppressant properties of the polystyrene (PS)-functionalized GO nanocomposite. They found that PS-functionalized GO nanocomposite presented better thermal stability than the pure PS, including greater char yields and higher initial and maximum decomposition temperatures [11]. More recently, Yuan at al. functionalized GO with 9,10-dihydro-9-oxa-10-phosphaphenanthrene-10-oxide (DOPO) and cage octaminopropyl silsesquioxane to be added as the flame retardant material into polypropylene [20].

Among conventional halogen-free flame retardants, phosphorus-based flame retardants, by forming a good char barrier layer, show higher flame retardancy influences. Thus, two-dimensional compounds containing phosphorus could be potentially more effective flame retardants than other 2-D inorganic nanomaterials such as bare graphene and LDHs. Inspired by this idea, for the first time, 2-D iron hydroxyl phosphate (IP) nanostructure was demonstrated as a novel, low cost, and highly effective flame retardant and smoke suppressant for the PAN nanocomposite. Therefore, we designed a mild synthesis route for the preparation of 2-D IP nanostructure. Sheet-like IP nanomaterial was synthesized using a one-step and facile solvothermal method by means of iron (II) sulfate heptahydrate, ethylene glycol, and phosphoric acid. Furthermore, the influence of the synthesized IP with a 2-D structure on the thermal stability, flammability as well as fire hazard of the PAN/IP nanocomposite was thoroughly investigated. The FE-SEM image of the PAN/IP nanocomposite exhibited absence of holes and cracks which proved suitable interaction and dispersion of the IP within the matrix. It was found that the peak heat release rate of the PAN/IP nanocomposite was decreased by 25.5%. Also, the total smoke release and the CO production rate of the PAN/IP nanocomposite were decreased by 28.0 and 63.0%, respectively.

EXPERIMENTAL

Materials

All materials were purchased from Merck Company and used as they received. The materials included iron(II) sulfate heptahydrate ($FeSO_4.7H_2O$, 99%), ethylene glycol (99.5%), phosphoric acid (H_3PO_4, 85%), ammonia (NH_3, 25%), dimethyl sulfoxide (DMSO, 99%) and absolute ethanol. PAN granules were composed of 93.5 wt% acrylonitrile and 6.5 wt% methylacrylate that were prepared from Polyacryl Iran Public Corporation, Isfahan, Iran.

Synthesis of sheet-like IP nanostructure

The IP nanosheet was synthesized through the solvothermal process. First, 1.4 g of $FeSO_4.7H_2O$ was added into 60.0 mL of ethylene glycol/deionized water mixture (50:50 wt/wt%) under magnetic stirring condition at room temperature. Second, 0.25 mL H_3PO_4 was dropwise added to

the previous solution (under stirring) to obtain a transparent solution. Third, 3.0 mL of NH_3 was introduced into the above solution and finally, after 20 min stirring, the obtained solution was poured to a 100 mL Teflon-lined, stainless steel autoclave and sealed. Then, it was heated for 2 h at 200 °C in oven (heating ramp was 10 °C/min). After that, the autoclave was naturally cooled down to the ambient conditions. The resultant product was centrifuged for 20 min at 10000 rpm, washed three times by distilled water, absolute ethanol, and acetone, respectively. Subsequently, the product was dried for 7 h at 50 °C to achieve the resulting powder.

Preparation of the PAN/IP nanocomposite

The PAN/IP nanocomposite was obtained through the solution casting technique. For this purpose, the IP (0.1 g) was introduced into DMSO solution (40.0 mL) and subjected to ultrasonic irradiation (for 30 s) to achieve a homogeneous mixture. Then, PAN powder (5.0 g) was added to the mixture under strong stirring at 70 °C. After 2 h, a viscose homogeneous mixture was obtained that was casted and dried for 24 h at 100 °C. For comparison, pure PAN film was also casted under identical conditions without adding any IP nanosheets.

Characterization

The X-ray photoelectron spectrum (XPS) was obtained to examine the composition/binding properties of the sample surface using Kratos Axis Ultra DLD spectrometer using an Al-K as the X-ray source that was operated at 1486.6 eV. The X-ray diffraction (XRD) patterns were achieved using INEL EQUINOX 3000 X–ray diffractometer by Cu Kα radiation, λ=1.5406 Å, with 2θ=5-70° to study the phase and crystallinity of each sample [21]. The transmission electron microscopy (TEM) images were attained on HITACHI HT7700 instrument (software version was 02/05). The surface morphology and particle size were investigated by means of field emission scanning electron microscope (FE-SEM), Mira3 FE-SEM, TESCAN, Czech Republic. The elemental mapping images were obtained with an energy-dispersive X-ray analyzer, Oxford Instrument, England to investigate the distributions of elements within the sample [22, 23]. The Raman spectra were provided on P50C0R10 laser Raman spectrometer with excitation wavelength of 532 nm using Nd : YAG laser, TEKSAN Co. The Fourier-transform infrared (FT-IR) spectra were taken using Equinox 55 Bruker spectrometer in the wavenumber range of 400–4000 cm^{-1} [24]. The thermogravimetric analysis (TGA) was accomplished by TGA Q5000 IR thermogravimetric analyzer, TA instruments, with 20 °C/min heating ramp under air condition. The UL-94 vertical burning analysis was performed based on ASTM D3801 for samples of 130×13×1.6 mm^3 dimensions. The combustion analysis was done by a cone calorimeter, FTT, UK, according to ISO 5660 on specimens (with 100×100×3 mm^3 dimensions) that were wrapped within aluminum foils and horizontally exposed to external 35 kW/m^2 heat flux.

RESULTS AND DISCUSSION

The IP characterization

The XRD technique was used to study the crystallinity and phase purity of materials [25]. The XRD pattern of the as-prepared IP sample is presented in Fig. 1a. The peaks located at 2θ = 18.1, 26.9, 28.0, 34.3, 39.6 and 44.4° can be indexed to the (101), (103), (004), (201), (203) and (204) planes of $Fe_3(PO_4)_2(OH)_2$, respectively [26, 27]. Also, the weak peaks at 2θ = 20.4 and 22.6° are assigned to the (211) and (112) planes of $FePO_4.2H_2O$, respectively, that are in agreement with the standard XRD pattern for the $FePO_4.2H_2O$ [27]. The XRD pattern confirms that crystalline and pure $Fe_3(PO_4)_2(OH)_2$ material is successfully synthesized by the solvothermal method.

Morphology of a material can be studied using the FE-SEM micrograph [28]. Figs. 1b1 and Fig. 1b2 illustrate the FE-SEM images of the IP. It can be seen that the synthesized IP has a sheet-like morphology with a thickness of about 40 nm. In addition, elemental mapping analysis (Fig. 1c) obviously indicates homogenous distribution of the O, P and Fe elements within the IP sample. The TEM image was obtained to more exactly study the morphology and particle size of the as-prepared IP (Fig. 1d). The result demonstrates that the IP has a sheet-like morphology which is expected to be favorable for the flame retardancy application [16].

The FT-IR spectrum of the IP provides information about the presence of expected functional groups and components in the sample (Fig. 2a). The absorption peak at 3435 cm^{-1} is related to the stretching vibration of hydroxyl (O-H) bonds and adsorbed water, indicating the O–H groups

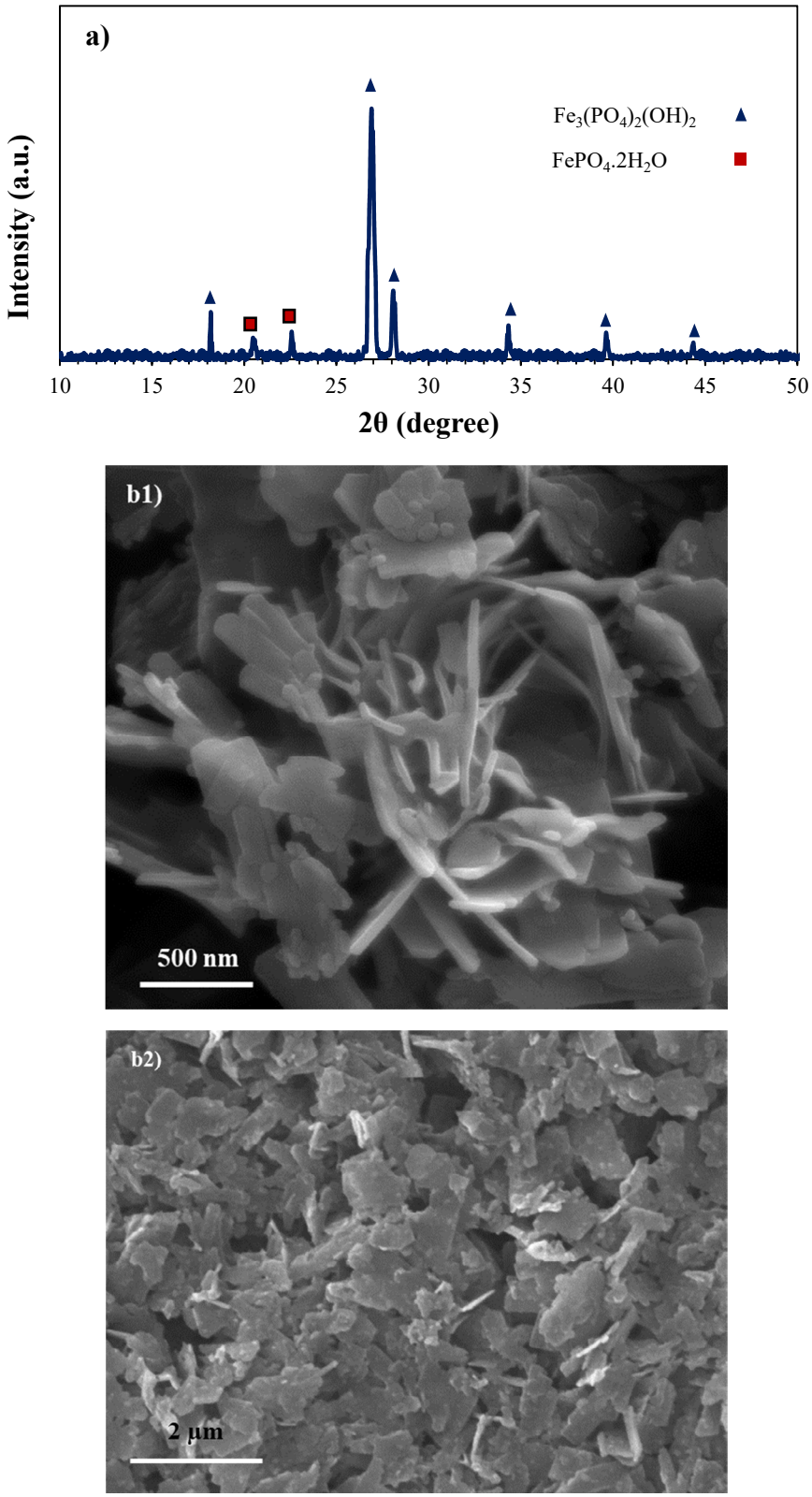

Fig. 1. (a) XRD pattern, (b) FE-SEM image, (c) elemental mapping images, and (d) TEM image of the as-prepared IP.

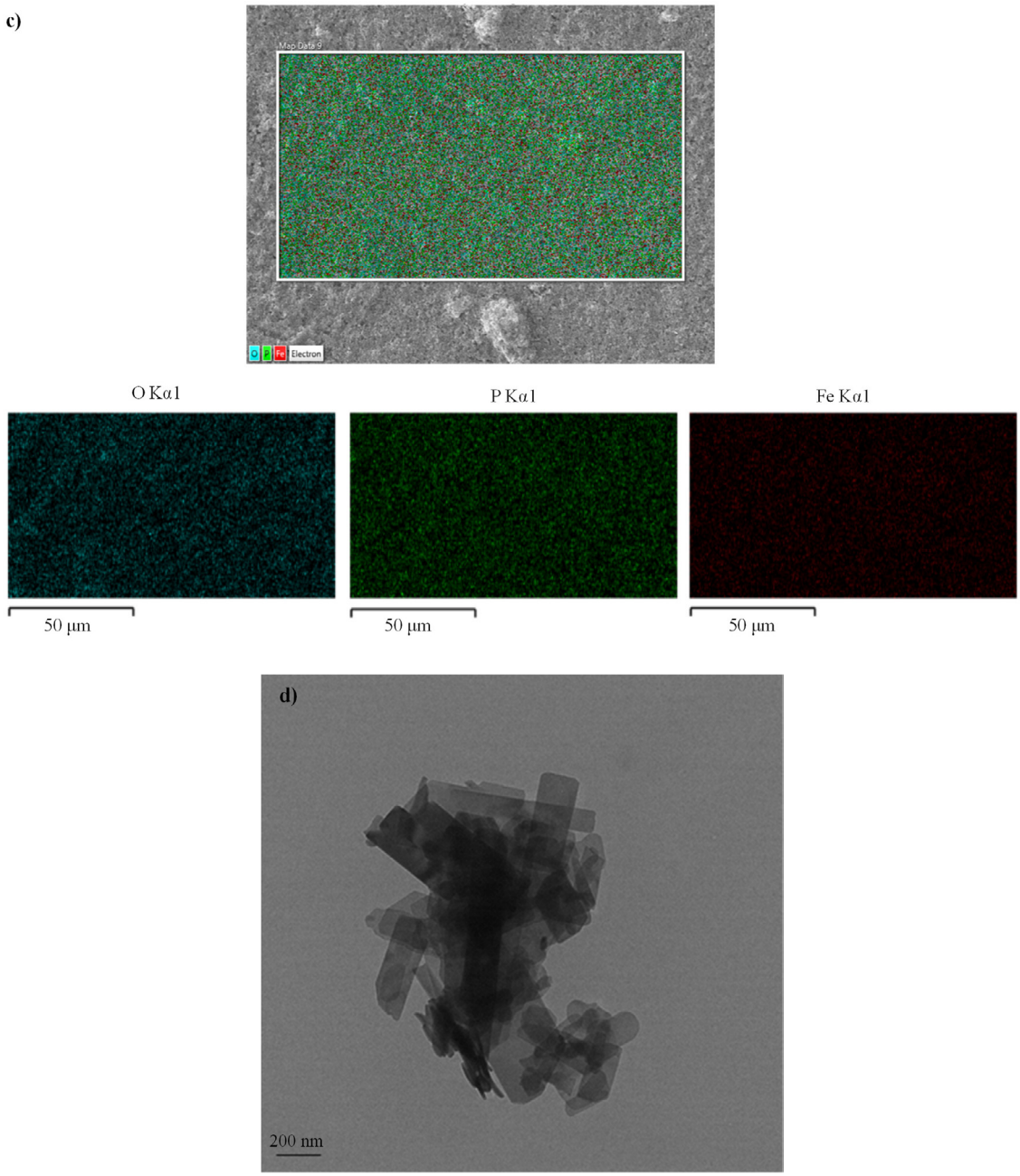

Continued Fig. 1. (a) XRD pattern, (b) FE-SEM image, (c) elemental mapping images, and (d) TEM image of the as-prepared IP.

exist in the structure of IP [29-31]. Furthermore, the band located at 1635 cm^{-1} corresponds to the water H-O-H symmetric bending mode [32]. The characteristic bands of PO_4^{3-} anions are observed at about 1068, 1144, 1046, 998, 628 and 545 cm^{-1} [27] and the band at 430 cm^{-1} is correlated to the vibrational stretching mode of the Fe-O bonds. Besides, the weak absorption peaks at 2920 and 2880 cm^{-1} are associated with the stretching vibrations of C-H bonds in the $–CH_3$ and $–CH_2$ groups, which can be due to the solvent residuals [27].

The surface composition of the IP was explored using the XPS analysis. The survey XPS spectrum of the IP (Fig. 2b) shows peaks located at about 135, 287, 533, and 720 eV which are assigned to

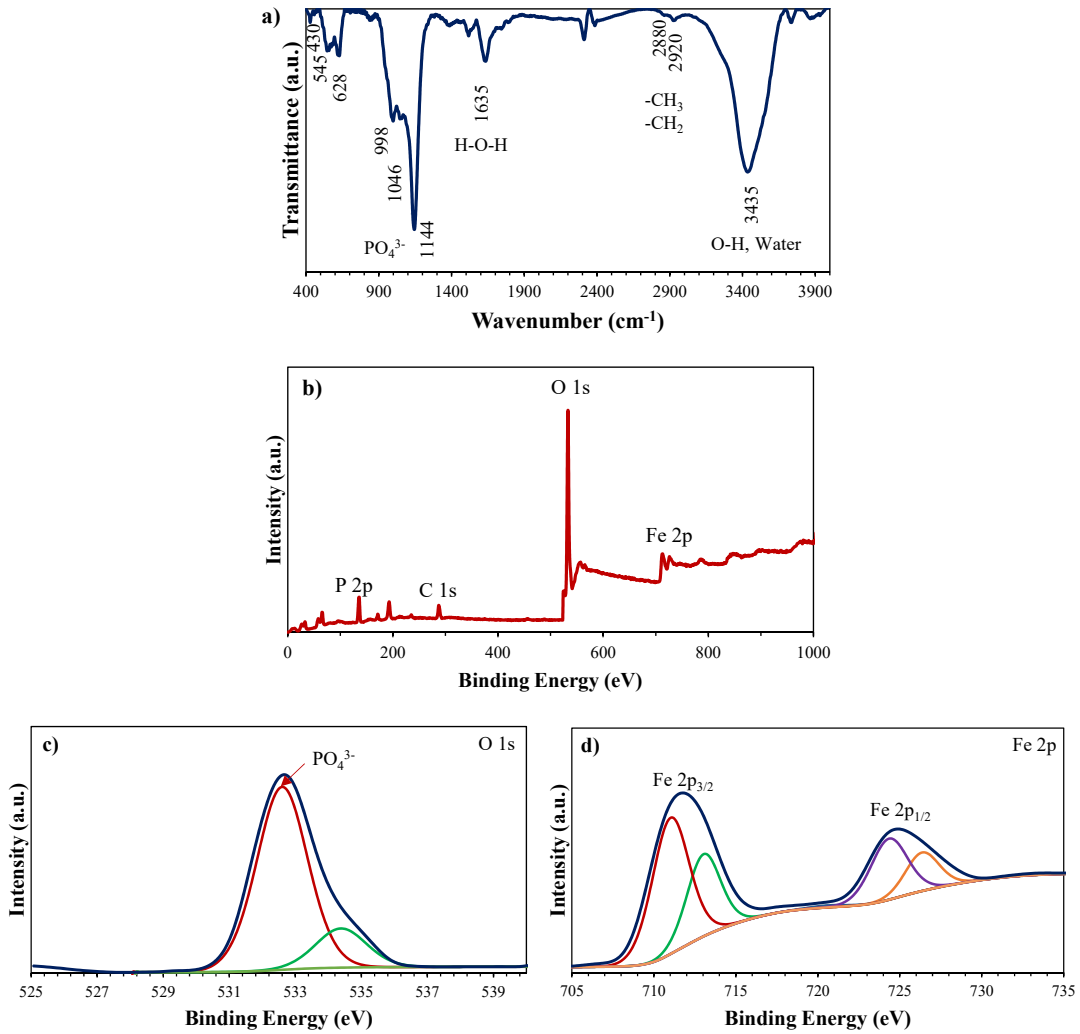

Fig. 2. (a) The FTIR spectra, (b) XPS survey spectrum, (c) O 1s XPS high resulotion spectrum, and (d) Fe 2p XPS high resulotion spectrum of the as-prepared IP.

the P 2p, C 1s, O 1s and Fe 2p characteristic peaks, respectively [26, 29]. Thus, the sample contains the P, O, Fe, and C elements and the C element can be originated from the atomsphere and/or solvent. The high-resolution O 1s XPS spectrum of the IP (Fig. 2c) is divided into two peaks observed at 532.6 and 534.2 eV. The main peak at 532.6 eV is ascribed to the oxygen atoms of $(PO_4)^{3-}$ groups, while the peak at 534.2 eV binding energy is attributed to other phosphorus containing species existing on the sample surface [29]. The high resolution Fe 2p spectrum for the IP (Fig. 2d) displays two spin–orbit doublets (Fe^{2+} and Fe^{3+}) and two shakeup satellites. The peaks situated near 713 and 727 eV are associated with the Fe^{2+}, and the peaks at approximately 711 and 724 eV are attributed to Fe^{3+} cations [26]. The XPS results confirm the XRD pattern, elemental mapping, and FT-IR spectrum and clearly illustrate that the $Fe_3(PO_4)_2(OH)_2$ has successfully been synthesized.

Thermal and fire properties of the PAN/IP and PAN

Figs. 3a and 3b exhibit the FE-SEM micrographs of the pure PAN and PAN/IP nanocomposite, respectively, giving indirect evidence of homogeneous distribution of the IP in the PAN matrix. Holes and cracks on the surface of the nanocomposite are genereally formed due to the nanostructure agglomeration and/or weak intractions between polymer matrix and

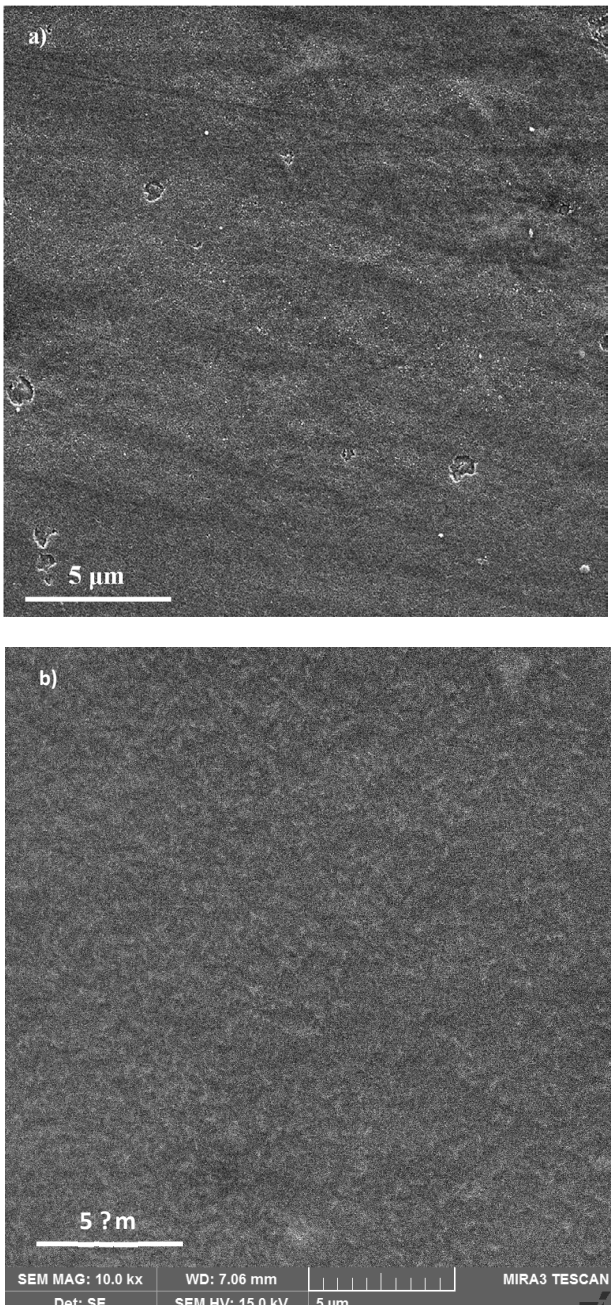

Fig. 3. The FE-SEM images of (a) the neat PAN and (b) the PAN/IP nanocomposite.

nanostructure [33]. The absence of such holes and cracks thus indicates good interactions and adequate dispersion of the IP in the matrix. The uniform dispersion of the IP within the polymer is very imperative for achieving good flame retardant properties [34].

The TGA plots were achieved for the PAN/IP nanocomposite and pure PAN to investigate their thermal decomposition behaviors. The TGA and DTG diagrams for the pure PAN and the nanocomposite in air condition are presented in Figs. 4a and 4b, respectively. It is seen that the degradations of the PAN and PAN/IP nanocomposite include three steps. The first step occurs in the temperature range of 100-200 °C so that 2-3% (for the pure PAN) and 6-7% (for the

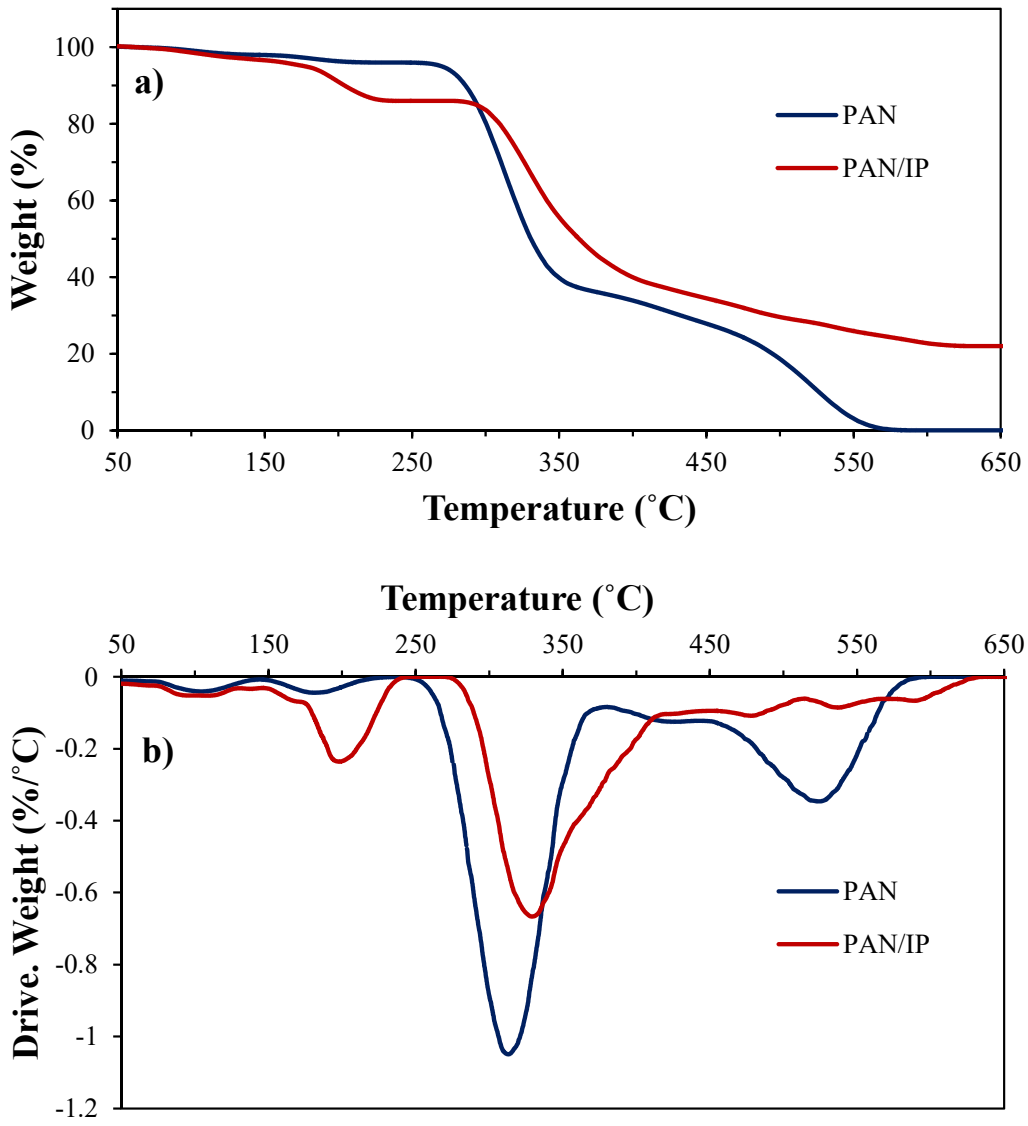

Fig. 4. (a) The TGA and (b) DTG curves of the neat PAN and the PAN/IP nanocomposite under air atmosphere.

PAN/IP) weight losses occur that are probably due to elimination of small molecules (such as H_2O and DMSO) [35, 36] as well as the hydroxyl moieties existing on the IP surface [3, 27, 37, 38]. The first step of the weight loss indicates that the IP can release water molecules (through the elimination of hydroxyl groups) at temperatures around 200 °C. This is an endothermic process that can act as a heat sink and improve the flame retardancy of the IP [39]. In addition, gaseous H_2O molecules are non-flammable which can dilute the flammable gases and further enhance the IP flame retardancy features [40]. The second phase includes the maximum weight loss which occurs in the temperature range of 300-400°C and ascribed to the oligomerization of nitrile and losing additional gaseous volatile compounds [3, 4].

The DTG plots of the PAN/IP nanocomposite and pure PAN were taken to examine their thermal stability [41]. The DTG profiles (Fig. 4b) indicate that the second step of weight loss in the pure PAN and PAN/IP samples takes place at 313 and 330 °C, respectively, which illustrates addition of the IP into the PAN matrix delays the thermal decomposition and accordingly enhances the PAN thermal stability. Besides, the DTG curves prove that the PAN/IP has a lower weight loss rate/intensity compared to that of the neat PAN.

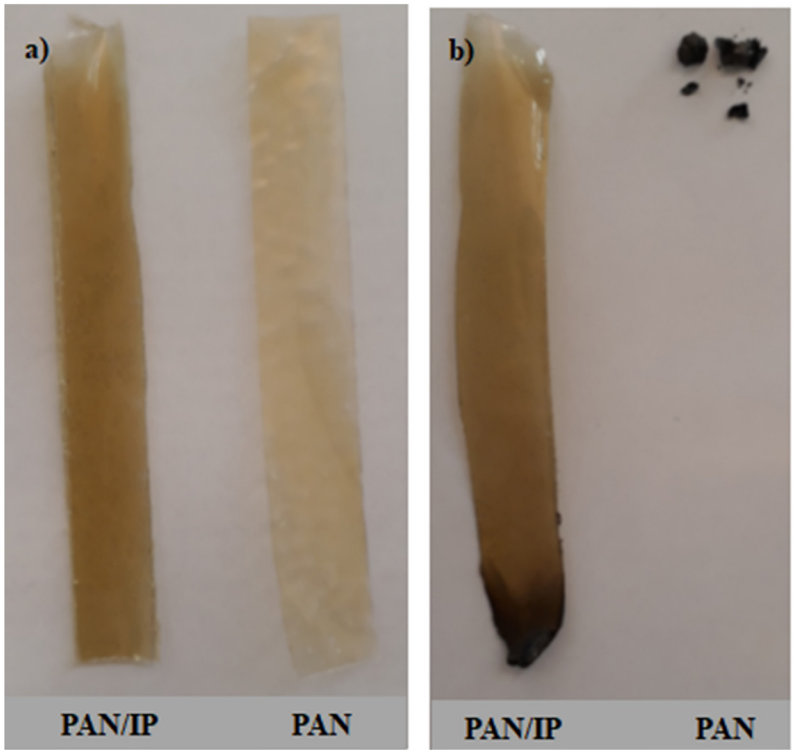

Fig. 5. The images of the neat PAN and PAN/IP nanocomposite (a) before and (b) after vertical UL-94 test.

Such results may be assigned to the influence of the IP that increases the char layer strength and therefore creates a protecting barrier layer over the surface of the PAN/IP composite [12, 16]. The char layer acts as a physical barrier to hinder the transfer of mass/heat between the gaseous and condensed phases [8, 16]. As a result, the polymer composite can be more slowly degraded. Moreover, phosphorus catalyzes the carbonization process that enhances the char layer quantity thereby further delays the polymeric sample degradation [14]. This hypothesis is confirmed as the PAN/IP composite reveals a lower weight loss. The last degradation phase is happened within 500-600 °C temperature range that is related to the pyrolysis of the PAN polymer [3]. The TGA diagram displays that the PAN pyrolysis is complete as it is disappeared at temperatures lower than 600 °C without remaining any residual char. Conversely, ~23% residual char is achieved at temperatures >600 °C for the PAN/IP sample confirming the IP has a catalytic influence in the carbonization reaction that is advantageous to decrease the fire hazards of material [42]. Large quantity of strong char layer serves as the barrier to interfere with the transfer of both heat (from the heat source onto the material) and mass (from the material toward the flame) during the combustion of the PAN/IP polymeric nanocomposite [16].

The influence of the IP on the PAN flame retardancy characteristic is examined by means of vertical UL-94 burning test. Figs. 5a and 5b show the digital images of the neat PAN and PAN/IP materials, respectively, before and after performing the UL-94 experiment. It is found that the pure PAN is very flammable as it fiercely burns along with dripping upon ignition and this causes the fire spreading that is a fire hazard [43]. The neat PAN is rapidly and continuously burnt in ~40 s till it is completely burnt out and only a little quantity of light brittle char is formed. Addition of the IP significantly improves the flame retardancy property of the PAN/IP nanocomposite placing it in V-0 category. Incorporation of the IP in the polymer matrix may increase the strength of the obtained char layer and thus, by forming a barrier layer on the surface of the polymer, the process of mass and heat transfers is disrupted and eventually, the flame is extinguished [44, 45].

Several factors can contribute in the flame

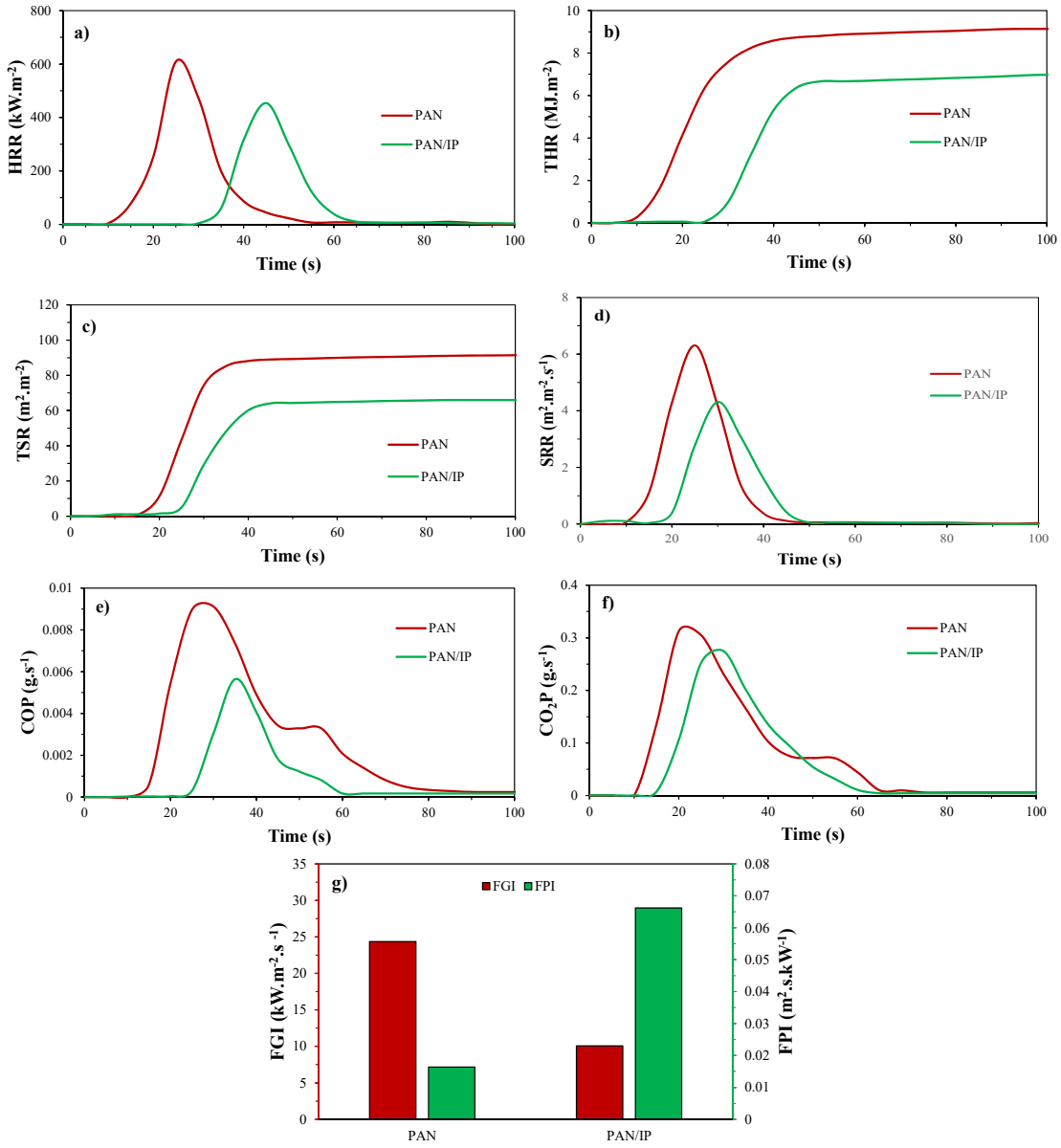

Fig. 6. (a) HRR, (b) THR, (c) TSR, (d) SRR, (e) COP, (f) CO_2P curves, and (g) fire hazards evaluation of neat PAN and PAN/IP nanocomposite.

retardancy property of a material. The FE-SEM image of the PAN/IP (Fig. 3b) indicates that the IP nanosheets are well-dispersed in the PAN matrix, which is one key factor in improving the flame retardancy effect [15]. Besides, incorporation of the IP in the PAN matrix may increase the strength (acting as a reinforcing agent) and amount (due to the catalyzing role of the phosphorous in the carbonization process) of the obtained char layer which was clearly revealed by the TGA. Thus, the barrier layer formed over the polymer surface disrupts the heat and mass transfer processes during the PAN/IP nanocomposite combustion and ultimately the flame is quenched [14, 16]. Moreover, the sheet-like morphology of the IP may further improve the protective properties of the char barrier layer.

The influence of the IP on the PAN combustion features has been investigated by cone calorimetry analysis. Fig. 6 illustrates the results which include time to ignition (t_{ign}), total smoke release (TSR), total heat release (THR), heat release rate (HRR),

Table 1. Cone calorimeter data of the neat PAN and the PAN/IP nanocomposite at 35 $kW.m^{-2}$.

Sample	t_{ign} (s)	t_{PHRR} (s)	PHRR ($kW.m^{-2}$)	THR ($MJ.m^{-2}$)	COY ($kg.kg^{-1}$)	CO_2Y ($kg.kg^{-1}$)	TSR ($m^2.m^{-2}$)	FPI ($m^2.s.kW^{-1}$)	FGI ($kW.m^{-2}.s^{-1}$)
PAN	10	25	609	9.1	0.08	2.6	89.0	0.016	24.4
PAN/IP	30	40	453	6.6	0.03	2.0	64.2	0.066	10.1

CO production rate (COP) and CO_2 production rate. Also, Table 1 provides the cone calorimeter data for the PAN and the PAN/IP measured at 35 kW/m^2. Fig. 6a shows that incorporation of the IP into the PAN matrix decreases the PHRR by 25.5% from PAN to PAN/IP. Furthermore, it is delayed by approximately 20 s. The postponed and lower PHRR may be associated with the effects of two parameters. First, the IP incorporated into the polymer matrix may act as a reinforcing material, which enhances the obtained char layer strength. Also, formation of the barrier layer over the polymer surface disrupts the mass and heat transfer processes throughout the combustion of the PAN/IP nanocomposite [8, 11]. Second, phosphorous catalyzes the carbonization route leading to a more efficient barrier influence [11]. The protective properties can be further improved by the sheet-like morphology of the IP. Similar to the HRR, the THR (Fig. 6b) is diminished by identical mechanisms.

Figs. 6c and 6d show the TSR and smoke release rate (SRR) curves, respectively. Smoke is composed of a mixture of gases in addition to liquid and solid particles that is emitted while a material is combusted and/or pyrolyzed. A protective char layer, which does not allow solid particles, vapors and gases to pass through can thus reduce the TSR [46, 47]. This could explain the reduction of TSR by about 28% for the PAN/IP in comparison to that of the neat PAN. Figs. 6e and 6f illustrate the CO and CO_2 production rate curves, respectively. Results emphasize that the total CO yield (COY) of the PAN/IP decreases by about 63% relative to that of the pure PAN which is associated with the IP catalytic effect on the CO oxidation and char creation [3, 11, 48]. In addition to the COY, the total CO_2 yield (CO_2Y) also decreases by 23% as compared to that of the PAN. This phenomenon is mainly assigned to the influence of the sheet-like IP containing char layer which disrupts the processes of mass and heat transfer and eventually decreases the release of combustible and non-combustible volatiles. The fire performance index (FPI, $\frac{t_{ign}}{PHRR}$) and the fire growth index (FGI, $\frac{PHRR}{t_{PHRR}}$) can be employed to further analyze the fire hazards [43]. Therefore, if the FPI is larger or the FGI is smaller, a lower fire hazard is measured. The data in Fig. 6g approve that the fire safety of the nanocomposite sample has significantly been improved which is suggested to be caused by the proficient barrier influence of the IP.

Residual char characterization

The residual char microstructures produced by the neat PAN and the PAN/IP nanocomposites are studied by their FE-SEM micrographs that are presented in Fig. 7. It is observed in Fig. 7a that the char related to the pure PAN has several holes over the surface that are correlated to exhausting the combustion gaseous products [17]. Nevertheless, the residual char of the PAN/IP (Fig. 7b) reveals that adding IP into the PAN increases the char homogeneity and therefore cracks and holes do not exist on the surface. It is known that the presence of the cracks and holes over the barrier char layer surface prevents the protective layer to show its effective influence [17]. Accordingly, transfer of mass (e.g. combustible gases and O_2) and heat into the protective layer can easily be happened. This has been supported by the appearance of spheres in Fig. 7b. These spheres are associated with the gas molecules captured by the char layer. Thus, the pure PAN is quickly burnt out that leaves behind only few char but the PAN/IP nanocomposite shows favorable flame retardency features. Such data support the findings attained in the TGA and the UL-94 test.

Fig. 7c demonstrates the Raman spectra for the residual chars produced by the pure PAN and the PAN/IP. The Raman spectra illustrate two sharp peaks at about 1590 and 1360 cm^{-1}. The former peak located at 1590 cm^{-1} (G band) is assigned to the existence of ordered graphitic carbon [11]. The latter peak observed at 1360 cm^{-1} (D band) is related to the formation of amorphous carbon [11]. Graphitization degree of residual char is accounted for using the I_G/I_D ratio that corresponds to the ratio of their related peak areas. Fig. 7c shows that the I_G/I_D value enhances

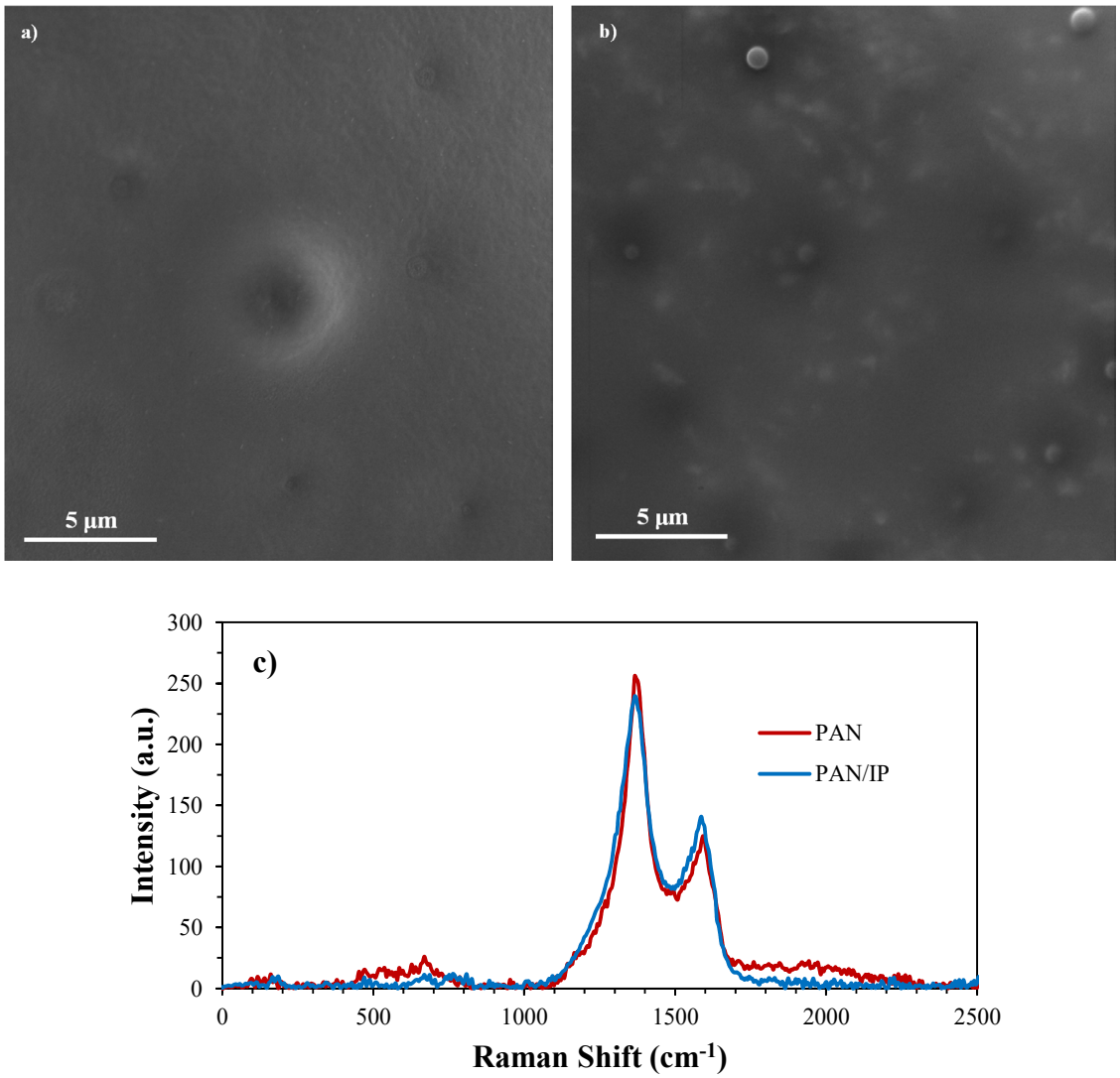

Fig. 7. (a, b) the FE-SEM images of the residual chars of neat PAN and PAN/IP nanocomposite, and (c) the Raman spectra of the residual chars of the neat PAN and PAN/IP nanocomposite.

from 0.49 (in the neat PAN) to 0.59 (in the PAN/IP), which indicates incorporation of the IP in the PAN matrix enhances the degree of graphitization in the char residue and accordingly the quality of the char layer is amended giving further support for the ability of the PAN/IP to create a protective char layer.

CONCLUSIONS

The IP nanosheets were synthesized through a facile solvothermal method and demonstrated as an efficient flame retardant and smoke suppressant material for the PAN. The IP significantly enhanced the thermal stability and deferred the thermal decomposition of the PAN. According to the UL-94 test results, it was found that incorporating the IP nanosheets into the PAN matrix enhanced its flame retardancy as the PAN/IP nanocomposite belonged to the V-0 group. The cone calorimetry data proved that introducing the IP nanosheets into the PAN decreased the PHRR by 25.5%, COP by 63%, and TSR by 28% as compared to those of the neat PAN. These substantial improvements in the flame retardancy and decrease in the fire hazards of the PAN/IP were attributed to the formation of a more uniform and stronger char layer as well as the nanosheet-like morphology of the IP, which were supported by the TGA diagrams of the PAN

and the PAN/IP as well as the FE-SEM images and the Raman spectra of the remaining chars. Thus, it can be concluded that the synthesized IP improved the flame retardancy and thermal stability of the PAN mainly through the condensed phase of action, which was based on the physical barrier layer, protecting the polymer form heat and flame.

ACKNOWLEDGEMENT

The financial support of this work by Research Office of Amirkabir University of Technology (Tehran Polytechnic) is gratefully acknowledged.

CONFLICTS OF INTEREST

The authors do not have any conflicts of interest.

REFERENCES

1. Wang D., Zhang Q., Zhou K,. Yang W., Hu Y., Gong X., (2014), The influence of manganese–cobalt oxide/graphene on reducing fire hazards of poly (butylene terephthalate). *J. Hazard. Mater.* 278: 391-400.
2. Haghighi Poshtiri A., Taghiyari H. R., Naghi Karimi A., (2013), The optimum level of nano-wollastonite consumption as fire-retardant in poplar wood (Populus nigra). *Int. J. Nano Dimens.* 4: 141-151.
3. Zhou K., Gui Z., Hu Y., (2016), The influence of graphene based smoke suppression agents on reduced fire hazards of polystyrene composites. *Composite- A: Appl. Sci. Manufact.* 80: 217-227.
4. Dong Y., Gui Z., Hu Y., Wu Y., Jiang S., (2012), The influence of titanate nanotube on the improved thermal properties and the smoke suppression in poly (methyl methacrylate). *J. Hazard. Mater.* 209: 34-39.
5. Yan X., Zhou W., Zhao X., Xu J., Liu P., (2016), Preparation, flame retardancy and thermal degradation behaviors of polyacrylonitrile fibers modified with diethylenetriamine and zinc ions. *J. Therm. Anal. Calorim.* 124: 719-728.
6. Chen X., Liu L., Jiao C., (2015), Influence of iron oxide brown on smoke suppression properties and combustion behavior of intumescent flame-retardant epoxy composites. *Adv. Polym. Technol.* 34: 21516-21521.
7. Asadi S. Z., Shekarian E., Tarighaleslami A. H., (2015), Preparation and characterization of nano-porous Polyacrylonitrile (PAN) membranes with hydrophilic surface. *Int. J. Nano Dimens.* 6: 217-226.
8. Ren Y., Jiang L., Tian T., Liu X., Han Z., (2018), Durable flame retardant polyacrylonitrile fabric via UV-induced grafting polymerization and surface chemical modification. *RSC Adv.* 8: 41389-41396.
9. Rahimi-Aghdam T., Shariatinia Z., Hakkarainen M., Haddadi-Asl V., (2020), Nitrogen and phosphorous doped graphene quantum dots: Excellent flame retardants and smoke suppressants for polyacrylonitrile nanocomposites. *J. Hazard. Mater.* 381: 121013-121018.
10. Rahimi-Aghdam T., Shariatinia Z., Hakkarainen M., Haddadi-Asl V., (2019), Polyacrylonitrile/N, P co-doped graphene quantum dots-layered double hydroxide nanocomposite: Flame retardant property, thermal stability and fire hazard. *Eur. Polym. J.* 120: 109256-109262.
11. Hu W., Yu B., Jiang S.-D., Song L,. Hu Y., Wang B., (2015), Hyper-branched polymer grafting graphene oxide as an effective flame retardant and smoke suppressant for polystyrene. *J. Hazard. Mater.* 300: 58-66.
12. Shariatinia Z., Javeri N., Shekarriz S., (2015), Flame retardant cotton fibers produced using novel synthesized halogen-free phosphoramide nanoparticles. *Carbohydr. Polym.* 118: 183-198.
13. Wang D.-Y., Liu X.-Q., Wang J.-S., Wang Y.-Z., Stec A. A ., Hull T. R., (2009), Preparation and characterisation of a novel fire retardant PET/α-zirconium phosphate nanocomposite. *Polym. Degrad. Stab.* 94: 544-549.
14. Zhang Y., Ren Y., Liu X., Huo T., Qin Y., (2018), Preparation of durable flame retardant PAN fabrics based on amidoximation and phosphorylation. *Appl. Surf. Sci.* 428: 395-403.
15. Sang B., Li Z.-w., Li X.-h., Yu L.-g., Zhang Z.-j., (2016), Graphene-based flame retardants: a review. *J. Mater. Sci.* 51: 8271-8295.
16. Wang X., Kalali E. N., Wan J.-T., Wang D.-Y., (2017), Carbon-family materials for flame retardant polymeric materials. *Prog. Polym. Sci.* 69: 22-46.
17. Shi Y., Yu B., Duan L., Gui Z., Wang B., Hu Y., Yuen R. K., (2017), Graphitic carbon nitride/phosphorus-rich aluminum phosphinates hybrids as smoke suppressants and flame retardants for polystyrene. *J. Hazard. Mater.* 332: 87-96.
18. Wang S., Hu Y., Zong R., Tang Y., Chen Z., Fan W., (2004), Preparation and characterization of flame retardant ABS/montmorillonite nanocomposite. *Appl. Clay Sci.* 25: 49-55.
19. Gao Y., Wu J., Wang Q., Wilkie C. A., O'Hare D., (2014), Flame retardant polymer/layered double hydroxide nanocomposites. *J. Mater. Chem. A*. 2: 10996-11016.
20. Yuan G., Yang B., Chen Y., Jia Y., (2019), Synthesis of a novel multi-structure synergistic POSS-GO-DOPO ternary graft flame retardant and its application in polypropylene. *Compos. - A: Appl. Sci. Manuf.* 117: 345-356.
21. Setoudeh N., Jahani S., Kazemipour M., Foroughi M. M., Hassani Nadiki H., (2020), Zeolitic imidazolate frameworks and cobalt-tannic acid nanocomposite modified carbon paste electrode for simultaneous determination of dopamine, uric acid, acetaminophen and tryptophan: Investigation of kinetic parameters of surface electrode and its analytical performance. *J. Electroanal. Chem.* 863: 114045-114051.
22. Foroughi M. M., Jahani S., Aramesh-Boroujeni Z., Rostaminasab Dolatabad M., Shahbazkhani K., (2021), Synthesis of 3D cubic of Eu^{3+}/Cu_2O with clover-like faces nanostructures and their application as an electrochemical sensor for determination of antiretroviral drug nevirapine. *Ceram. Int.* 47: 19727-19736.
23. Foroughi M. M., Jahani S., Aramesh-Boroujeni Z., Vakili Fathabadi M., Hashemipour Rafsanjani H., Rostaminasab Dolatabad M., (2021), Template-free synthesis of ZnO/Fe3O4/Carbon magnetic nanocomposite: Nanotubes with hexagonal cross sections and their electrocatalytic property for simultaneous determination of oxymorphone and heroin. *Microchem. J.* 170: 106679-106685.
24. Yinhua D., Foroughi M. M., Aramesh-Boroujeni Z., Jahani S., Peydayesh M., Borhani F, Khatami M., Rohani M., Dusek M., Eigner V., (2020), The synthesis, characterization, DNA/BSA/HSA interactions, molecular modeling, antibacterial

properties, and in vitro cytotoxic activities of novel parent and niosome nano-encapsulated Ho(iii) complexes. *RSC Adv.* 10: 22891-22908.
25. Foroughi M. M., Ranjbar M., (2017), Microwave-assisted synthesis and characterization photoluminescence properties: a fast, efficient route to produce ZnO/GrO nanocrystalline. *J. Mater. Sci.: Mater. Electron.* 28: 1359-1363.
26. Yang Q., Lu S., Shen B., Bao S., Liu Y., (2018), An iron hydroxyl phosphate microoctahedron catalyst as an efficient peroxidase mimic for sensitive and colorimetric quantification of H_2O_2 and glucose. *New J. Chem.* 42: 6803-6809.
27. Yu Y-D, Zhu Y-J., Wu J., (2017), Glycerin-assisted solvothermal synthesis of $Fe_3(PO_4)_2(OH)_2$ microspheres. *Mater. Lett.* 205: 158-161.
28. Hajmalek S., Jahani S., Foroughi M. M., (2021), Simultaneous voltammetric determination of tramadol and paracetamol exploiting glassy carbon electrode modified with $FeNi_3$ nanoalloy in biological and pharmaceutical media. *Chem. Select* 6: 8797-8808.
29. Song H., Sun Y., Jia X., (2015), Hydrothermal synthesis of iron phosphate microspheres constructed by mesoporous polyhedral nanocrystals. *Mater. Charact.* 107: 182-188.
30. Sarguru Nanajundaiah R., Hosur Kumara C., Madanahalli Ankanathappa S., (2022), Surface, structural and optical investigation on Poly Vinyl Alcohol (PVA)/Bi_2WO_6 nanocomposite films. *Int. J. Nano Dimens.*, 10.22034/ijnd.2022.1946867.2109
31. Jafarian Z., Nikpassand M., Pourahmad A., Zare Fekri L., (2022), Synthesis of fused Azo-linked 1, 2, 4-Triazole-3-Thione derivatives using Ag_2S/RHA-MCM-41 nanocomposite. *Int. J. Nano Dimens.* 13: 117-125.
32. Li S., Liu X., Mi R., Liu H., Li Y., Lau W.-M., Mei J., (2014), A facile route to modify ferrous phosphate and its use as an iron-containing resource for $LiFePO_4$ via a polyol process. *ACS Appl. Mater. Interf*. 6: 9449-9457.
33. Dittrich B., Wartig K.-A., Hofmann D., Mülhaupt R., Schartel B., (2013), Flame retardancy through carbon nanomaterials: Carbon black, multiwall nanotubes, expanded graphite, multi-layer graphene and graphene in polypropylene. *Polym. Degrad. Stab.* 98: 1495-1505.
34. Ghiyasiyan-Arani M., Masjedi-Arani M., Ghanbari D., Bagheri S., Salavati-Niasari M., (2016), Novel chemical synthesis and characterization of copper pyrovanadate nanoparticles and its influence on the flame retardancy of polymeric nanocomposites. *Sci. Rep.* 6: 25231-25238.
35. Gudarzifar H., Rezvani A., Sabbaghi S., (2021), Morphological investigation of Graphene Oxide/Polyacrylamide super-elastic nanocomposite by a solution polymerization process with enhanced rheological property and thermal conductivity. *Int. J. Nano Dimens.* 12: 20-36.
36. Ghobadi E., Hemmati M., Khanbabaei G., Shojaei M., Asghari M., (2015), Effect of nanozeolite 13X on thermal and mechanical properties of Polyurethane nanocomposite thin films. *Int. J. Nano Dimens.* 6: 177-181.
37. Phuruangrat A., Thongtem T., Thongtem S., (2010), Preparation and characterization of nano-crystalline $LiNi_{0.5}Co_{0.5}VO_4$ by tartate precursor combustion method. *Int. J. Nano Dimens.* 1: 111-118.
38. Kardam A., Rohit Raj K., Srivastava S., (2012), Novel nano cellulosic fibers for remediation of heavy metals from synthetic water. *Int. J. Nano Dimens.* 3: 155-162.
39. Ren Y., Zhang Y., Gu Y., Zeng Q., (2017), Flame retardant polyacrylonitrile fabrics prepared by organic-inorganic hybrid silica coating via sol-gel technique. *Progr. Org. Coat.* 112: 225-233.
40. Porter D., Metcalfe E., Thomas M., (2000), Nanocomposite fire retardants: A review. *Fire Mater.* 24: 45-52.
41. Abdi Z., Sedaghat S., (2016), Synthesis and characterization of functionalized single - walled carbon nanotube/chitosan/polyaniline nanocomposite. *Int. J. Nano Dimens.* 7: 25-32.
42. Pethsangave D. A., Khose R. V., Wadekar P. H., Some S., (2017), Deep eutectic solvent functionalized graphene composite as an extremely high potency flame retardant. *ACS Appl. Mater. Interf.* 9: 35319-35324.
43. Zhou K., Gui Z., Hu Y., Jiang S., Tang G., (2016), The influence of cobalt oxide–graphene hybrids on thermal degradation, fire hazards and mechanical properties of thermoplastic polyurethane composites. *Compos- A: Appl. Sci. Manuf.* 88: 10-18.
44. Yin Z., Cai W., Lu J., Yu B., Wang B., Song L., Hu Y., (2022), Cost-effective graphite felt and phosphorous flame retardant with extremely high electromagnetic shielding. *Compos. B Eng.* 236: 109819-109825.
45. Shi X.-H., Li X.-L., Li Y.-M., Li Z., Wang D.-Y., (2022), Flame-retardant strategy and mechanism of fiber reinforced polymeric composite: A review. *Compos. B. Eng.* 233: 109663-109671.
46. Shi Y., Long Z., Yu B., Zhou K., Gui Z., Yuen R. K., Hu Y., (2015), Tunable thermal, flame retardant and toxic effluent suppression properties of polystyrene based on alternating graphitic carbon nitride and multi-walled carbon nanotubes. *J. Mater. Chem. A* 3: 17064-17073.
47. Qiu Y., Qian L., Feng H., Jin S., Hao J., (2018), Toughening effect and flame-retardant behaviors of phosphaphenanthrene/phenylsiloxane bigroup macromolecules in epoxy thermoset. *Macromolec.* 51: 9992-10002.
48. Li M., Wu Z., Ma Z., Schwartz V., Mullins D. R, Dai S., Overbury S. H., (2009), CO oxidation on Au/$FePO_4$ catalyst: Reaction pathways and nature of Au sites. *J. Catal.* 266: 98-105.